analytical chemistry

Article

pubs.acs.org/ac

Impact of Adsorption on Scanning Electrochemical Microscopy Voltammetry and Implications for Nanogap Measurements

Sze-yin Tan,[†,‡] Jie Zhang,[‡] Alan M. Bond,[‡] Julie V. Macpherson,[†] and Patrick R. Unwin*[,†]

[†]Department of Chemistry, University of Warwick, Coventry, West Midlands CV4 7AL, United Kingdom

[‡]School of Chemistry, Monash University, Clayton, Victoria 3800, Australia

Supporting Information

ABSTRACT: Scanning electrochemical microscopy (SECM) is a powerful tool that enables quantitative measurements of fast electron transfer (ET) kinetics when coupled with modeling predictions from finite-element simulations. However, the advent of nanoscale and nanogap electrode geometries that have an intrinsically high surface area-to-solution volume ratio realizes the need for more rigorous data analysis procedures, as surface effects such as adsorption may play an important role. The oxidation of ferrocenylmethyl trimethylammonium ($FcTMA^+$) at highly oriented pyrolytic graphite (HOPG) is used as a model system to demonstrate the effects of reversible reactant adsorption on the SECM response. Furthermore, the adsorption of $FcTMA^{2+}$ species onto glass, which is often used to encapsulate ultramicroelectrodes employed in SECM, is also found to be important and affects the voltammetric tip response in a nanogap geometry. If a researcher is unaware of such effects (which may not be readily apparent in slow to moderate scan voltammetry) and analyzes SECM data assuming simple ET kinetics at the substrate and an inert insulator support around the tip, the result is the incorrect assignment of tip−substrate heights, kinetics, and thermodynamic parameters. Thus, SECM kinetic measurements, particularly in a nanogap configuration where the ET kinetics are often very fast (only just distinguishable from reversible), require that such effects are fully characterized. This is possible by expanding the number of experimental variables, including the voltammetric scan rate and concentration of redox species, among others.

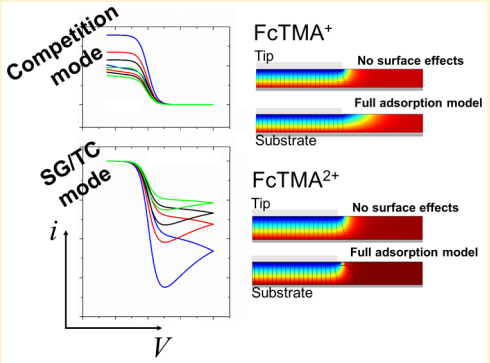

A long-term interest in electrochemistry has been the measurement of increasingly fast electron transfer (ET) kinetics at electrode/electrolyte interfaces to gain deeper fundamental understanding of heterogeneous interfacial ET.[1−3] Although considerable insight on interfacial ET can be gained from immobilized redox systems,[4−8] the overwhelming majority of studies deal with soluble redox species, which have to diffuse to and from the electrode. An important aspect to the study of fast ET kinetics in such systems is the need for high mass transport rates, so that this does not completely limit the current.[9−12] The introduction of ultramicroelectrode (UME) techniques from the 1980s onward has offered many advantages including reduced ohmic effects, fast response times, and high mass transport rates under both steady-state and transient conditions.[13,14] Hydrodynamic UMEs[10,11,15,16] and, particularly, the development of scanning electrochemical microscopy (SECM)[9,12,17,18] provide even higher mass transport rates under steady-state conditions.

In SECM ET kinetic measurements, a UME is positioned near a second (substrate) working electrode and both electrodes are biased externally to investigate the potential-dependent ET kinetics at one of the two electrode/electrolyte interfaces. High mass transport conditions prevail due to the shuttling of the oxidized and reduced forms of the redox couple between the two electrodes. With diffusion-limited redox shuttling (diffusion coefficient, D), the steady-state mass transport coefficient, k_t, becomes a function of tip−substrate separation, d ($k_t \sim D/d$),[19] so that high mass transport rates are obtained by decreasing the UME size and tip−substrate distances. This has fueled the trend of miniaturizing electrochemical systems, leading to the development of nanoelectrodes[20−26] and various nanogap systems.[27−33]

When using nanoscale electrochemical systems for quantitative kinetic measurements, precise knowledge of electrode geometry and the physicochemical characteristics of electrochemical cells is imperative. For example, unaccounted for irregularities in the electrode shape from idealized models,[34] tip recession,[35−37] or "lagooned" geometries[38,39] may produce highly erroneous determination (overestimation) of ET kinetic parameters.[40] Significant efforts have thus aimed at developing easy and reproducible electrode preparation procedures and better means of geometric characterization.[35,39,41−43] In this context, well-defined nanostructures such as graphene oxide flakes,[20] carbon nanotubes,[23−26,44] and nanowires[25,44,45] are attractive in that the geometry of the electrodes, as used, can often be characterized by techniques such as atomic force

Received: December 12, 2015
Accepted: February 13, 2016
Published: February 13, 2016

DOI: 10.1021/acs.analchem.5b04715
Anal. Chem. 2016, 88, 3272−3280

microscopy, and related methods. Beyond the precise geometric characterization of nanoscale electrodes, an intrinsic property of nanogap electrochemical cells is the very high surface area-to-solution volume ratio within (semi-)confined geometries. In this situation, even the weak adsorption of redox-active species may have a profound impact on the electrochemical response.

The significance of adsorption in nanogap cells has been reported by Lemay et al. using lithographically fabricated nanometer wide thin-layer electrochemical cells (TLCs).[30,46−49] In this configuration, two planar electrodes (electron-beam evaporated metal thin films) are used to create high surface area-to-solution volume ratio nanogap electrochemical cells and electrochemical correlation spectroscopy enables the investigation of the redox cycling of small populations of molecules. It has been found that simple outer-sphere redox molecules such as $[Ru(NH_3)_6]^{3+}$ and 1,1-ferrocene dimethanol adsorb at Pt electrodes and play a role in limiting the electrochemical response time,[30,46] dominate noise properties[47] and, at low solute concentrations, decrease current fluctuations[48,49] in these cells. Early TLC studies also considered the effect of redox adsorption on electrode materials in dual electrode cells with gaps on the approximately micrometer to ∼10 μm scale.[50−52] A significant difference between TLCs and SECM is that TLC studies never consider the insulator that encapsulates the electrode and are limited to redox cycling (feedback) experiments. A significant advantage of SECM, particularly substrate voltammetry SECM that we consider extensively herein, is the versatility to determine thermodynamic and kinetic properties at a plethora of electrode materials, such as graphene,[53] highly oriented pyrolytic graphite, HOPG,[28] and carbon nanotubes,[44] that would be difficult to fabricate into the TLC configuration.

In this work, we show how adsorption can greatly affect SECM voltammetric experiments, as well as highlighting how SECM can be used to reveal and quantify adsorption in electrochemical systems, building on earlier SECM adsorption studies in other situations.[19] The focus is ferrocenylmethyl trimethylammonium, $FcTMA^+$, which undergoes an apparently simple one-electron oxidation and has been used to study a wide range of electrode materials as an example of a fast outer-sphere redox couple.[28,32] However, it has also been demonstrated that ferrocene and its derivatives can adsorb onto electrode surfaces.[30,48,49,54,55] The substrate voltammetry configuration of SECM[27,28] is used to probe the adsorption and electrochemistry of $FcTMA^+$ at HOPG electrodes, a system that has received recent attention as one with apparently ultrafast kinetics.[28] The unequal diffusivities of $FcTMA^+$ and its oxidized form, $FcTMA^{2+}$, are carefully considered as this significantly affects the steady-state limiting current magnitudes measured in SECM[56,57] and nanogap configurations.[27,29] Lastly, we apply our findings to typical nanoscale SECM geometries and discuss the impact of electrode and glass adsorption on the SECM voltammetric response and the effect on kinetic and thermodynamic parameters deduced from such measurements.

THEORY AND SIMULATIONS

COMSOL Multiphysics 4.4 (COMSOL, AB, Stockholm, Sweden) finite-element method modeling was used to solve the time-dependent mass transport problem in a 2D-axisymmetric cylindrical SECM geometry (Figure 1a). The following diffusion equation applies throughout:

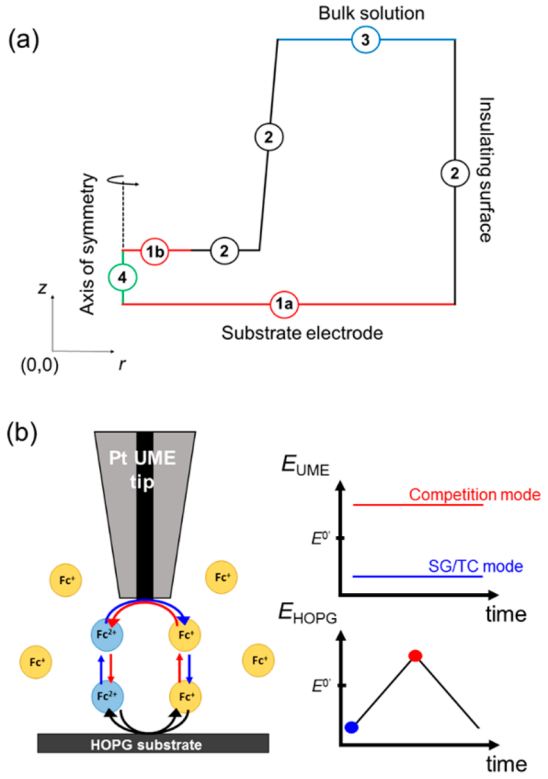

Figure 1. (a) Schematic (not to scale) of the 2D-axisymmetric SECM simulation domain and (b) diagram of the experimental protocols for substrate voltammetry SECM.

$$\frac{\partial c_i}{\partial t} = D_i\left(\frac{\partial^2 c_i}{\partial r^2} + \frac{1}{r}\frac{\partial c_i}{\partial r} + \frac{\partial^2 c_i}{\partial z^2}\right) \quad (1)$$

where c_i and D_i represent the concentration and diffusion coefficient of the redox species, i ($FcTMA^+$ or $FcTMA^{2+}$) and r and z are the radial distance from the center and the normal distance to the electrode, respectively.

The following redox process is considered at the HOPG substrate electrode:

$$FcTMA^+_{soln} \underset{k_{red,HOPG}}{\overset{k_{ox,HOPG}}{\rightleftharpoons}} FcTMA^{2+}_{soln} + e^- \quad (2)$$

where $k_{ox,HOPG}$ and $k_{red,HOPG}$ are the first-order heterogeneous oxidation and reduction rate constants given by the Butler−Volmer relationship:

$$k_{ox,HOPG} = k^0{}_{HOPG}\exp[(1-\alpha)f\eta_{HOPG}] \quad (3)$$

$$k_{red,HOPG} = k^0{}_{HOPG}\exp[-\alpha f\eta_{HOPG}] \quad (4)$$

where $k^0{}_{HOPG}$ is the standard rate constant for the $FcTMA^{+/2+}$ process at the HOPG substrate, α is the transfer coefficient (assumed reasonably to be 0.5), and $f = \frac{F}{RT}$ is a collection of constants where F is the Faraday constant, R is the universal gas constant, and T is the absolute temperature. $\eta_{HOPG} = E_{HOPG}(t) - E^{0\prime}$, is the overpotential; E_{HOPG} is the potential applied to the HOPG substrate electrode and $E^{0\prime}$ is the formal potential of the redox couple.

The adsorption of $FcTMA^+$ on HOPG is assumed to be reversible:

DOI: 10.1021/acs.analchem.5b04715
Anal. Chem. 2016, 88, 3272−3280

$$\mathrm{FcTMA^+_{soln}} \underset{k_{des,HOPG}}{\overset{k_{ads,HOPG}}{\rightleftharpoons}} \mathrm{FcTMA^+_{ads}} \quad (5)$$

where $k_{ads,HOPG}$ and $k_{des,HOPG}$ are the adsorption and desorption rate constants, respectively, such that the equilibrium adsorption constant is

$$K_{ads,HOPG} = \frac{k_{ads,HOPG}}{k_{des,HOPG}} \quad (6)$$

The flux of $FcTMA^+$ at the HOPG/electrolyte interface (Figure 1a, label 1a) depends on the ET process and adsorption:

$$-\mathbf{n}\cdot\mathbf{N}_{FcTMA^+,HOPG} = -k_{ox,HOPG}c_{FcTMA^+} + k_{red,HOPG}c_{FcTMA^{2+}} - \frac{\partial\theta_{HOPG}\Gamma^0{}_{HOPG}}{\partial t} \quad (7)$$

$FcTMA^{2+}$ does not adsorb appreciably at the HOPG electrode (vide infra), so only the ET kinetics are important:

$$-\mathbf{n}\cdot\mathbf{N}_{FcTMA^{2+},HOPG} = k_{ox,HOPG}c_{FcTMA^+} - k_{red,HOPG}c_{FcTMA^{2+}} \quad (8)$$

where $\mathbf{n}$ is the unit normal vector to the substrate surface, while $\mathbf{N}_{FcTMA^+,HOPG}$ and $\mathbf{N}_{FcTMA^{2+},HOPG}$ represent the flux of the reduced and oxidized species to the substrate electrode surface. θ_{HOPG} is the fraction of occupied adsorption sites on the HOPG surface, and $\Gamma^0{}_{HOPG}$ is the monolayer surface concentration of $FcTMA^+$ (5×10^{-10} mol cm^{-2}).[54]

The amount of $FcTMA^+$ adsorbed is assumed to follow a Langmuir isotherm:

$$\theta_{HOPG} = \frac{K_{ads,HOPG}c_{FcTMA^+}}{1 + K_{ads,HOPG}c_{FcTMA^+}} \quad (9)$$

The following redox process is considered at the UME tip surface:

$$\mathrm{FcTMA^+_{soln}} \underset{k_{red,UME}}{\overset{k_{ox,UME}}{\rightleftharpoons}} \mathrm{FcTMA^{2+}_{soln}} + \mathrm{e^-} \quad (10)$$

The following Butler–Volmer relationship is applied:

$$k_{ox,UME} = k^0{}_{UME}\exp[(1-\alpha)f\eta_{UME}] \quad (11)$$

$$k_{red,UME} = k^0{}_{UME}\exp[-\alpha f\eta_{UME}] \quad (12)$$

where $k^0{}_{UME}$ is the standard rate constant for ET at the Pt UME, set high to ensure reversibility (25 cm s^{-1}).[22] $\eta_{UME} = E_{UME} - E^{0\prime}$, $E_{UME} \gg E^{0\prime}$ in the competition mode, and $E_{UME} \ll E^{0\prime}$ in the SG/TC mode, with E_{UME} fixed to drive the reaction of interest.

For $t > 0$, the redox flux at the Pt UME tip surface (Figure 1a, label 1b) is defined by

$$-\mathbf{n}\cdot\mathbf{N}_{FcTMA^+,UME} = \mathbf{n}\cdot\mathbf{N}_{FcTMA^{2+},UME} = -k_{ox,UME}c_{FcTMA^+} + k_{red,UME}c_{FcTMA^{2+}} \quad (13)$$

Other boundary conditions are shown in Figure 1a, where insulating surfaces (label 2) are described by $\mathbf{n}\cdot\mathbf{N}_{FcTMA^+} = \mathbf{n}\cdot\mathbf{N}_{FcTMA^{2+}} = 0$, the bulk solution boundary (label 3) is given by $c_{FcTMA^+} = c^0{}_{FcTMA^+}$ and $c_{FcTMA^{2+}} = 0$, and label 4 represents the axis of symmetry.

The substrate and tip current were calculated from

$$i_{HOPG} = 2\pi F\int_0^{a_{HOPG}} (-k_{ox,HOPG}c_{FcTMA^+} + k_{red,HOPG}c_{FcTMA^{2+}})r\,\mathrm{d}r \quad (14)$$

$$i_{UME} = 2\pi F\int_0^{a_{UME}} (-k_{ox,UME}c_{FcTMA^+} + k_{red,UME}c_{FcTMA^{2+}})r\,\mathrm{d}r \quad (15)$$

Typically, 100,000 triangular mesh elements were used in each simulation with the greatest mesh resolution at the electrode boundaries and edges where the concentration gradient is steepest.[58]

EXPERIMENTAL SECTION

Chemicals. Ferrocenylmethyl trimethylammonium hexafluorophosphate, $[FcTMA^+][PF_6^-]$ was synthesized in-house via an exchange reaction of $FcTMA^+I^-$ (Strem Chemicals, Ltd.) with $AgPF_6$ (Strem). KCl (99%) was purchased from Sigma-Aldrich and used without further purification. All solutions were prepared using high purity water (Millipore Corp. purification system), with a resistivity ca. 18.2 MΩ cm at 25 °C. A 1 M amount of KCl was added as the supporting electrolyte in all solutions.

Electrode Materials. A Pt disk macroelectrode (radius, a_{Pt} = 0.1 cm) was obtained from CH Instruments, Inc. A Pt disk UME was fabricated in-house using an established procedure,[59] involving heat sealing of a 12.5 μm radius microwire (Goodfellow, Huntingdon, U.K.) in a borosilicate glass capillary under vacuum. The microwire was connected with solder to a larger copper wire inserted into the capillary.[59] The end of the UME was polished flat and conically polished to obtain an RG value—ratio of the radius of the insulating glass sheath to that of the active electrode—of ca. 10. Prior to use, the UME was polished with an alumina slurry (0.05 μm) on a soft microfiber polishing pad (MicroCloth, Buehler Ltd.) and then on a clean wet microfiber pad, to produce the finished electrode surface. ZYA grade HOPG was acquired from GE Advanced Ceramics, Strongsville, OH, USA. The HOPG sample was placed on a silicon wafer, coated with chromium (2 nm) and gold (60 nm) using Acheson Electrodag (Agar Scientific, 1415M). An external electrical contact was created by lowering a metal pin onto the exposed gold surface using a micropositioner. Fresh HOPG basal surfaces were prepared by gently pressing down Scotch tape onto the sample and pulling-off the top layers, as reported extensively in the literature.[33,60−63]

Cyclic Voltammetry and SECM Instrumentation. Cyclic voltammetry (CV) was carried out for the oxidation of 0.4 mM $FcTMA^+$ (1 M KCl) in aqueous solution in a three-electrode configuration using a CHI 760C potentiostat (CH Instruments, Inc.) where an HOPG substrate, a Pt wire, and a AgCl-coated Ag wire were used as working, counter, and reference electrodes, respectively. The reference electrode was thus Ag/AgCl (1 M KCl). A 20 μL droplet of electrolyte solution was placed on the HOPG surface (area of ca. 0.165 cm^2) with the counter and reference electrodes placed into the droplet.[63] An advantage of this electrochemical cell is that it can be assembled and used within seconds of sample cleavage,[63] minimizing surface contamination.

An intermittent-contact (IC)-SECM setup was used for substrate voltammetry SECM measurements.[64,65] Salient details of tip positioning are given in Supporting Information (SI) section S-1. A four-electrode SECM configuration was adopted with the Pt UME tip and HOPG substrate as the working electrodes, and the same counter and reference electrodes as mentioned above. For this purpose a CHI 760C bipotentiostat

DOI: 10.1021/acs.analchem.5b04715
Anal. Chem. 2016, 88, 3272−3280

was used. Scan rates applied to the HOPG substrate ranged from 0.05 to 10 V s^{-1}. Potentials applied to the UME tip were either 0.8 V (to detect $FcTMA^+$ by diffusion-limited oxidation) or 0.1 V (to detect $FcTMA^{2+}$ by diffusion-limited reduction) for the competition (shielding) mode or SG/TC mode, respectively. A droplet configuration was also used in this case, and all measurements were made within 10 min of HOPG cleavage and droplet placement, such that evaporation of water from the electrolyte solution was negligible.

RESULTS AND DISCUSSION

Adsorption of $FcTMA^+$ on HOPG Electrodes. Macroscopic CVs for the oxidation of $FcTMA^+$ (0.4 mM in 1 M KCl) at HOPG in the droplet configuration[63] gave half-wave potentials, $E_{1/2,app}$ at 0.38 V (vs Ag/AgCl 1 M KCl) (Figure 2a). The peak-to-peak separation, ΔE_p values decreased

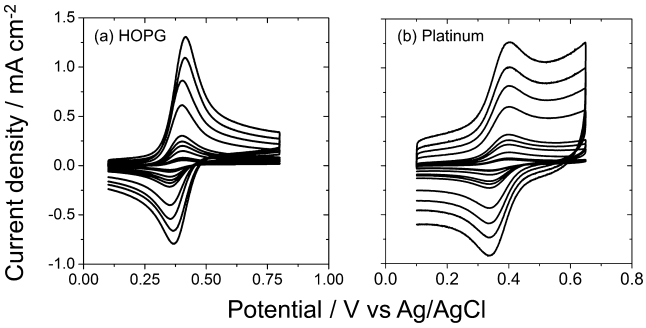

Figure 2. CVs for the one-electron oxidation of 0.4 mM $FcTMA^+$ in aqueous 1 M KCl supporting electrolyte at a (a) freshly cleaved ZYA grade HOPG and (b) platinum disk electrode at different scan rates (50 mV s^{-1} to 10 V s^{-1}).

monotonically from 51 mV at 0.05 V s^{-1} to 40 mV at 10 V s^{-1} (see SI section S-2 and Figure S-1a). These values are smaller than 57 mV, expected for purely diffusion-controlled voltammograms at 25 °C and seen for CVs for the oxidation of $FcTMA^+$ (0.4 mM in 1 M KCl) at a macroscopic Pt electrode (Figure 2b). Note the low background current for the voltammetry at HOPG compared to Pt due to the much lower capacitance of the HOPG/aqueous interface.[60] With further information presented below, these characteristics are indicative of a diffusional redox system that is complicated by ET from weakly adsorbed species.

The peak currents of the forward potential scan were larger than those of the reverse potential scan with the difference increasing with scan rate (see SI section S-2 and Figure S-1b). However, at low scan rates (<1 V s^{-1}), the ratio of forward to reverse peaks tends to 1 and ΔE_p only differs a small amount from the purely diffusional response (see above). Without running a wide range of scan rates and focusing on relatively slow scan speeds, one could mistake this process for one that only involves diffusion (no adsorption),[28] especially as electrode placement and supporting electrolyte concentration may be critical in determining ΔE_p in small volume (droplet) electrochemical cells.[63] Comparison of experimental to computed diffusional waves (using precise diffusion coefficients) showed that the experimental currents exceeded the simulated ones (see SI section S-2 and Figure S-1c), whereas the reverse scan voltammetry fit quite well. Thus, while $FcTMA^+$ adsorbs at the HOPG electrode, $FcTMA^{2+}$ that is produced does not adsorb appreciably and a significant proportion of $FcTMA^{2+}$ produced by the oxidation of adsorbed $FcTMA^+$ diffuses away from the electrode on this time scale.

This type of behavior has previously been reported for ferrocene and its derivatives on other electrode materials such as platinum[30] and glassy carbon,[54] but not recognized on HOPG.[28] As we show further herein, it is essential to acknowledge $FcTMA^+$ adsorption if one is to achieve accurate kinetic analysis. Examination of the macroscale droplet CVs, and the excess charge compared to a diffusional process,[55] allows us to estimate the $FcTMA^+$ surface coverage at the beginning of the experiment to be ca. 0.9 × 10^{-10} mol cm^{-2} (18%) for a bulk concentration of 0.4 mM $FcTMA^+$ (1 M KCl). For the purpose of the analysis herein, this is a reasonable estimate; a more accurate value results from SECM measurements (see below).

Substrate voltammetry SECM was employed for a quantitative analysis of the amount of $FcTMA^+$ adsorbed onto the HOPG surface. In this work, 0.4 mM $FcTMA^+$ (1 M KCl) was used throughout. The UME tip (radius, a_{UME} = 12.5 μm) was positioned at a fixed distance from the HOPG substrate surface and E_{HOPG} was scanned from 0.1 to 0.8 V (50 mV s^{-1}) to oxidize $FcTMA^+$ to $FcTMA^{2+}$. At E_{UME} = 0.8 V, the UME tip gives the positive feedback response (E_{HOPG} = 0.1 V). As the substrate potential is scanned positively, the UME tip competes with the substrate to oxidize $FcTMA^+$, and this is known as the competition mode.[66] In the substrate generation/tip collection mode (E_{UME} = 0.1 V), the tip current rises from zero as the UME tip collects $FcTMA^{2+}$ produced at the HOPG substrate electrode during the voltammetric sweep (Figure 1b). Hence, a pair of competition and SG/TC voltammograms at the same tip position can be taken at a set of tip–substrate separations to change the interelectrode mass transport rate and effective surface area-to-solution volume ratio, and thus the sensitivity of the system to adsorption compared to diffusion.

Panels a(i) and a(ii) of Figure 3 show four pairs of competition and SG/TC voltammograms (each pair measured at the same tip–substrate distance is shown in the same color) taken at different tip–substrate heights, d = 2.58, 3.71, 4.59, and

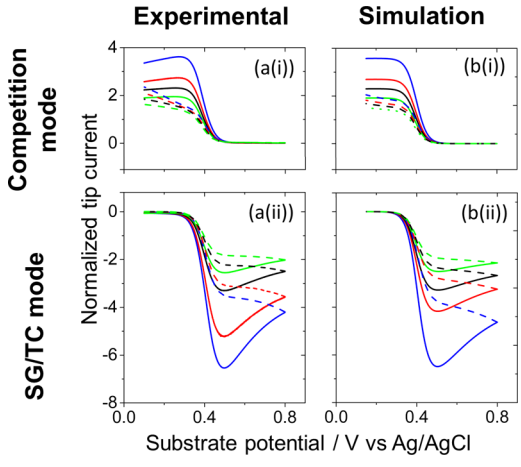

Figure 3. Experimental (a) and simulated (b) tip current–substrate potential curves for the competition and SG/TC modes for the one-electron oxidation of 0.4 mM $FcTMA^+$ in 1 M KCl supporting electrolyte in aqueous media at an HOPG surface (ZYA grade) at different normalized tip–substrate heights (L = 0.209 (blue), 0.297 (red), 0.367 (black), and 0.478 (green)) at 50 mV s^{-1}. Solid and dashed lines show the forward and reverse curves, respectively. Simulation parameters can be found in the text.

DOI: 10.1021/acs.analchem.5b04715
Anal. Chem. 2016, 88, 3272–3280

5.98 μm (determined from positive feedback limiting current at the beginning of the competition mode scan (discussed later)). Note that the substrate voltammograms were close to those seen without a tip present (see above). The tip currents were normalized with respect to the steady-state diffusion-limited tip current for the oxidation of $FcTMA^+$ in the bulk solution. Noticeably, the tip current measured in the competition mode was always smaller than its SG/TC counterpart, and, in both configurations, voltammograms deviate significantly from those expected for the adsorption-free voltammetric response (see SI section S-3 and Figure S-2b). This was especially noticeable for the SG/TC mode.

Simulated voltammograms considering $FcTMA^+$ adsorption onto the HOPG substrate electrode are shown in Figure 3b. The simulation parameters were as follows: k^0_{UME} = 25 cm s^{-1} (reversible), k^0_{HOPG} = 10 cm s^{-1} (reversible), α = 0.5, $E^{0\prime}$ = 0.38 V, D_{FcTMA^+} = 6.7 × 10^{-6} cm^2 s^{-1} (determined from steady-state voltammetry (see SI section S-4)), and $D_{FcTMA^{2+}}$ = 6.1 × 10^{-6} cm^2 s^{-1} (determined by SECM chronoamperometry in feedback and SG/TC mode (see SI section S-5)). The amount of adsorbed $FcTMA^+$ on the HOPG substrate was determined to be 1.13 × 10^{-10} mol cm^{-2} (22%) by comparison of experimental and simulated tip voltammograms, with most parameters fixed, and only those ($K_{ads,HOPG}$) relating to adsorption variable. Note that the adsorption of $FcTMA^+$ on platinum has previously been observed[30,32] and is not ruled out. However, it is undetectable under our experimental conditions, and the theoretical model assumes that adsorption at HOPG dominates, with negligible adsorption of $FcTMA^+$ at the Pt UME tip.

In the competition mode, as noted above, (see Figure 1b) the UME tip potential oxidized $FcTMA^+$ to $FcTMA^{2+}$ at a diffusion-limited rate, while the substrate potential was cycled between 0.1 and 0.8 V at 50 mV s^{-1}. The UME tip competition voltammograms show a typical diffusion-limited (positive feedback) current on the forward wave, indicated by the solid line (Figure 3a(i)). As the HOPG substrate potential was anodically scanned such that $FcTMA^+$ was oxidized to $FcTMA^{2+}$, the UME tip current decreased (competition with the substrate for $FcTMA^+$). Interestingly, by comparing simulations for all tip−substrate heights, the positive feedback limiting currents, measured with and without reactant adsorption on the substrate, give the same values (see SI section S-3 and Figure S-2a(i),b(i)). This is because the positive feedback limiting current merely depends on the redox competition between the substrate and tip electrodes for $FcTMA^+$ in solution. Hence, the experimental positive feedback UME tip limiting currents can be used to accurately determine the tip−substrate separations without complications from $FcTMA^+$ adsorption processes. However, even though simulations with and without $FcTMA^+$ adsorption on the substrate gave equivalent limiting currents, the $E_{1/2,app}$ values were shifted positively by 17, 13, 12, and 9 mV at d = 2.58, 3.71, 4.59, and 5.98 μm, respectively, compared to the diffusion only simulations. This is because $FcTMA^+$ adsorbed on the HOPG surface at the start of the voltammetric sweep is gradually released during the sweep, particularly in the later part of the voltammogram. Thus, adsorption of $FcTMA^+$ on the HOPG substrate subtly affects the voltammetric waveshape.

On the reverse competition mode potential scan, the currents are not retraceable (dashed lines in Figure 3a(i),b(i)) but the experimental and simulations are closely similar when adsorption of $FcTMA^+$ at the HOPG substrate is taken into account. This occurs due to $FcTMA^{2+}$ reconversion to $FcTMA^+$ at the HOPG substrate where the latter adsorbs. This accounts for the generally smaller UME tip current measured on the reverse substrate potential scan (0.8 to 0.1 V) in the competition mode. Without substrate adsorption of $FcTMA^+$, the forward and reverse tip current responses (with the substrate potential scan) are much closer; see SI section S-3 and Figure S-2.

In the SG/TC mode, the UME tip is used to amperometrically detect substrate-generated $FcTMA^{2+}$ as the HOPG substrate potential was cycled from 0.1 to 0.8 V at 50 mV s^{-1} to oxidize $FcTMA^+$ to $FcTMA^{2+}$. The resultant tip current−substrate potential curves are peak shaped (Figure 3a(ii),b(ii)), rather than the typical sigmoidal response observed for this mode without adsorption of $FcTMA^+$ at the substrate electrode (see SI section S-3 and Figure S-2b(ii)). An increase of UME tip current was observed as the substrate potential was anodically scanned, reaching a maximum value at a potential ∼ 0.49 V vs Ag/AgCl (1 M KCl) before decreasing as the substrate potential was further increased. The surplus of $FcTMA^+$ present on the HOPG substrate surface at the start of the voltammetric experiment results in a higher flux of $FcTMA^{2+}$ species to the tip surface during the anodic potential sweep. This is clear from panels a and b of SI section S-3 Figure S-3 which show the concentration profiles for $FcTMA^+$ in the tip−substrate gap at E_{HOPG} = 0.5 V (close to the peak potential) on the anodic sweep for the SG/TC mode without and with reactant adsorption on the substrate electrode. The concentration of $FcTMA^+$ near the UME tip is higher than the bulk concentration with $FcTMA^+$ adsorption at the substrate.

On the reverse cathodic sweep of the substrate potential, the measured UME tip currents are smaller and tend to resemble the steady-state diffusion-controlled response. This is because $FcTMA^+$ adsorption no longer affects the tip response. A comparison of SG/TC tip voltammogram simulations, with and without surface adsorption effects, can be found in SI section S-3 Figure S-2a(ii),b(ii), respectively. The substantial contribution from $FcTMA^+$ adsorption to the SG/TC tip current−substrate potential response is seen at all tip−substrate heights, with the effect increasingly significant at closer tip−substrate separations.

Since tip−substrate heights can be determined accurately from the positive feedback limiting current of the competition mode voltammetric response (see above), the magnitude of peak currents measured in the SG/TC mode can be fitted to provide accurate measurement of reactant ($FcTMA^+$) adsorption on the HOPG substrate when matched with simulations. Via this method, we estimated Γ_{HOPG} = 1.1 × 10^{-10} mol cm^{-2} at a bulk concentration of 0.4 mM $FcTMA^+$.

We next briefly investigated the effect of scan rate on substrate voltammetry SECM. Panels a and b of Figure 4 show typical experimental data and simulations for three pairs of competition and SG/TC mode tip responses taken at the same tip−substrate height (L = 0.209) but at different scan rates (50 mV s^{-1} and 0.1 and 0.5 V s^{-1}), indicated by the different colors. At higher scan rates, the surplus concentration of $FcTMA^{2+}$ generated at the HOPG surface (from adsorbed $FcTMA^+$) does not have sufficient time to diffuse out of the tip−substrate gap, where $t_{diff(escape)} \sim (a_{UME}RG)^2/D$. Hence, peak currents are no longer observed in the SG/TC mode at scan rates ≥ 0.5 V s^{-1}, but the current is massively enhanced compared to the adsorption-free case. Again, experiments and simulations are

DOI: 10.1021/acs.analchem.5b04715
Anal. Chem. 2016, 88, 3272−3280

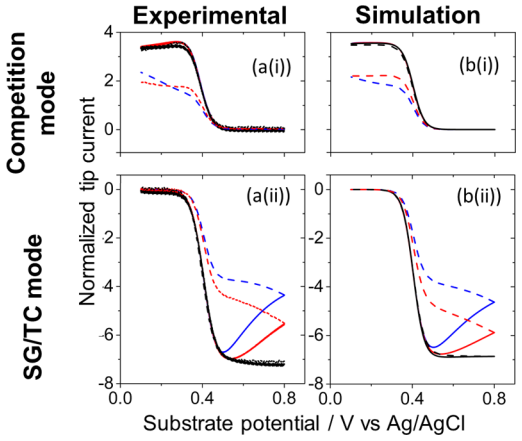

Figure 4. Experimental (a) and simulated (b) tip current−substrate potential curves for the competition and SG/TC modes for the one-electron oxidation of 0.4 mM $FcTMA^+$ in 1 M KCl supporting electrolyte in aqueous media at an HOPG surface (ZYA grade) at different scan rates (50 (blue), 100 (red), and 500 (black) mV s^{-1}) at L = 0.209. Solid and dashed lines show the forward and reverse curves, respectively. All other simulation parameters are identical to those used in Figure 3.

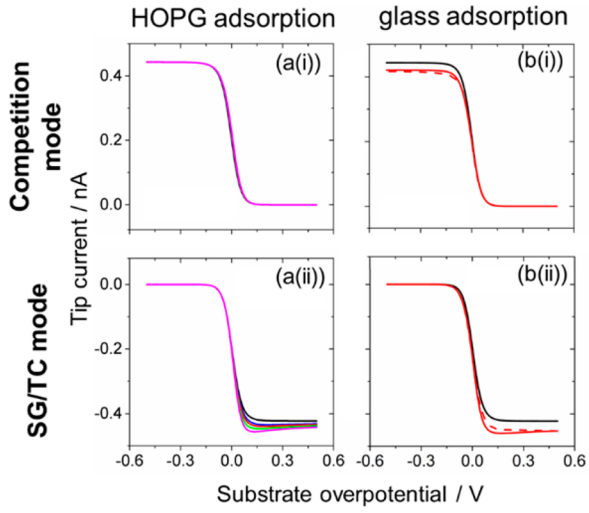

Figure 5. Simulated nanogap substrate voltammetry SECM tip current−substrate potential responses for (a) varying values of $\Gamma_{HOPG,FcTMA^+}$ (1.1×10^{-10} (22%), 1.53×10^{-10} (30%), 2.0×10^{-10} (40%), and 2.6×10^{-10} (50%) mol cm^{-2}) and (b) full adsorption model (red). In both parts, the black curves represent the adsorption-free tip response. Solid and dashed lines show the forward and reverse curves, respectively. Simulation parameters: L = 0.1, k^0 = 5 cm s^{-1}, ν = 50 mV s^{-1}, a_{UME} = 0.5 μm, RG = 2, α = 0.5, D_{FcTMA^+} = 6.7×10^{-6} cm s^{-1}, and $D_{FcTMA^{2+}}$ = 6.1×10^{-6} cm s^{-1}. Glass adsorption parameters are given by Γ^0_{glass} = 2.3×10^{-9} mol cm^{-2}, $K_{ads,glass}$ = 2.56×10^6 cm^3 mol^{-1}, and K_{12} = 9×10^6 M^{-1} s^{-1}.

in close agreement using only the adsorption parameters for $FcTMA^+$ as a variable.

Other Considerations and Impact on Nanogap Simulations. In light of our experimental results, we applied our findings to substrate voltammetry SECM at typical nanogap geometries[28] where a UME tip of a_{UME} = 0.5 μm with RG = 2 is held at typical normalized tip−substrate distances, L = 0.1−0.3. In absolute terms these are much smaller (50−150 nm) than those we employed above. Furthermore, the possibility of increased $FcTMA^+$ adsorption on the substrate due to prolonged exposure times (to air) and the adsorption of the redox couple on glass, commonly used to isolate the UME tip, will be considered. The following parameters apply throughout: k^0_{UME} = 25 cm s^{-1} (reversible),[22] α = 0.5, D_{FcTMA^+} = 6.7×10^{-6} cm^2 s^{-1} and $D_{FcTMA^{2+}}$ = 6.1×10^{-6} cm^2 s^{-1}, C_{FcTMA^+} = 0.4 mM, and $\Gamma^0_{HOPG,FcTMA^+}$ = 5.0×10^{-10} mol cm^{-2}.

Effect of $FcTMA^+$ Adsorbed on HOPG. Although most of the SECM measurements were taken within minutes of surface cleavage, it is also interesting to consider the impact of HOPG exposure to air. We have shown that the behavior of some redox couples changes significantly over time,[60,62,63] for a variety of reasons attributed to surface contamination, delamination, surface oxidation, and other factors, and it is also known that HOPG is susceptible to atmospheric contamination.[60] Some experiments, such as SECM measurements, where one has to assemble the HOPG sample in a cell before conducting the experiment, may result in unavoidable contamination of the surface, as well as damage to the sample from compression in a cell.[60] As shown in SI section S-6, the amount of $FcTMA^+$ adsorbed on HOPG increased to 2.0×10^{-10} mol cm^{-2} ($FcTMA^+$ bulk concentration of 0.4 mM) after 1 h exposure of a cleaved surface to air. Figure 5a shows simulated forward scan tip responses for the competition and SG/TC modes where $\Gamma_{HOPG,FcTMA^+}$ was systematically increased (1.1×10^{-10} (22%), 1.53×10^{-10} (30%), 2.0×10^{-10} (40%), and 2.6×10^{-10} (50%) mol cm^{-2}). Other simulation parameters include the following: L = 0.1 (50 nm) and k^0_{HOPG} = 5 cm s^{-1}. The black curves are the tip voltammetric response with no surface adsorption effects, for comparison. In this ideal case, it can be seen that the positive feedback limiting current (beginning of the competition mode scan) is larger than that of the SG/TC curve, which is expected because $FcTMA^{2+}$ has a smaller diffusion coefficient than $FcTMA^+$.[27,29,56,57] When there is $FcTMA^+$ adsorption on HOPG, the positive feedback limiting currents (Figure 5a(i)) remain unchanged from the control (adsorption-free) voltammogram (see earlier). Similar to the above microgap experiments, $E^{0\prime}$ values are positively shifted by 4 mV for all adsorption values considered.

In the SG/TC mode (Figure 5a(ii)), tip currents are larger than expected and increase as the amount of adsorbed $FcTMA^+$ is increased, due to the increased flux of $FcTMA^{2+}$ toward the SECM tip from the oxidation of substrate-adsorbed $FcTMA^+$. In this situation, the larger tip current enhancement would lead to an underestimation of tip−substrate distance (if adsorption was neglected by a researcher). Moreover, the tip voltammogram with adsorption is steeper, which would result in an overestimation of the kinetic parameter, k^0. When fitted to an adsorption-free analytical model, essentially reversible ($k^0_{app} \geq$ 14 cm s^{-1}) responses are found for all SG/TC curves, rather than k^0 = 5 cm s^{-1} that was actually applied to the simulations. Kinetic analyses for the voltammograms in Figure 5a are summarized in SI section S-9 Table S-1, where the simulated voltammograms with different amounts of $FcTMA^+$ adsorption on HOPG are analyzed as though they were adsorption-free (as a researcher might naively assume), and the resulting error in tip−substrate separation (underestimated), kinetics (overestimated), and thermodynamic parameter, $E^{0\prime}$, are revealed.

Adsorption of Redox-Active Species on Glass. UME voltammetry in a drop of solution was used to determine adsorption isotherms for $FcTMA^+$ and $FcTMA^{2+}$ at the solution−glass interface (SI section S-1).[67] The highly charged $FcTMA^{2+}$ species was found to adsorb strongly on glass

DOI: 10.1021/acs.analchem.5b04715
Anal. Chem. 2016, 88, 3272−3280

surfaces (see SI section S-7). In this part of the simulations, we thus modified the boundary condition on the glass that surrounds the UME tip to include $FcTMA^{2+}$ adsorption and the well-known fast lateral charge propagation that occurs within surface-attached redox molecules,[68−72] especially ferrocenes at high surface coverage.[72] A detailed description of the boundary condition applied can be found in SI section S-8.

Figure 5b shows simulated results that consider both $FcTMA^{+}$ adsorption on HOPG and $FcTMA^{2+}$ adsorption on glass. Again, for comparative purposes, the black curves show the limiting case of no adsorption on any surface. Within this framework, at the same tip−substrate distances, the positive feedback tip limiting currents (at the beginning of the competition mode potential scan) were always smaller than those in the SG/TC mode. This has previously been seen experimentally, and the anomalous limiting current magnitudes were attributed to the presence of an organic contaminant layer, which had selective charge permeability in favor of the $FcTMA^{+}$ species.[28] Evidently, a similar effect can be observed, at least qualitatively, by considering the known adsorption of $FcTMA^{+}$ on HOPG and $FcTMA^{2+}$ on the UME glass sheath.

The UME tip positive feedback limiting current obtained in the competition mode was always lower than the simulated adsorption-free counterpart. This is because the oxidation of $FcTMA^{+}$ by glass-bound $FcTMA^{2+}$ essentially "competes" with the oxidation of $FcTMA^{+}$ at the UME tip surface. This is evident by the shallower concentration gradient of $FcTMA^{+}$ at the tip−glass interface compared to the adsorption-free counterpart (Figure 6a). Conversely, a higher UME tip limiting

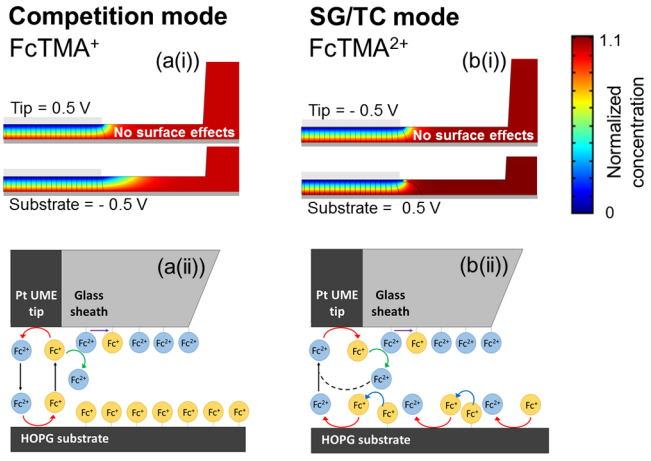

Figure 6. (i) Concentration profiles of (a) $FcTMA^{+}$ in the competition mode and (b) $FcTMA^{2+}$ in the SG/TC mode, with the parameters defined in Figure 5b. (ii) Illustrations of the redox adsorption processes occurring in the (a) competition and (b) SG/TC modes.

current is obtained for the SG/TC case compared to the simulated adsorption-free counterpart. This is because ET between the UME tip-generated $FcTMA^{+}$ and glass-bound $FcTMA^{2+}$ provides an additional "feedback" loop, which further enhances the flux of $FcTMA^{2+}$ to the UME tip surface on top of the above-mentioned increased flux of $FcTMA^{2+}$ due to the oxidation of substrate-adsorbed $FcTMA^{+}$ (Figure 6b).

Figure 7a shows results for systematically varied substrate kinetic values (k^0_{HOPG} = 0.5, 1.0, and 10 cm s^{-1}) at a fixed distance, L = 0.1 (50 nm) for the full adsorption model. For all

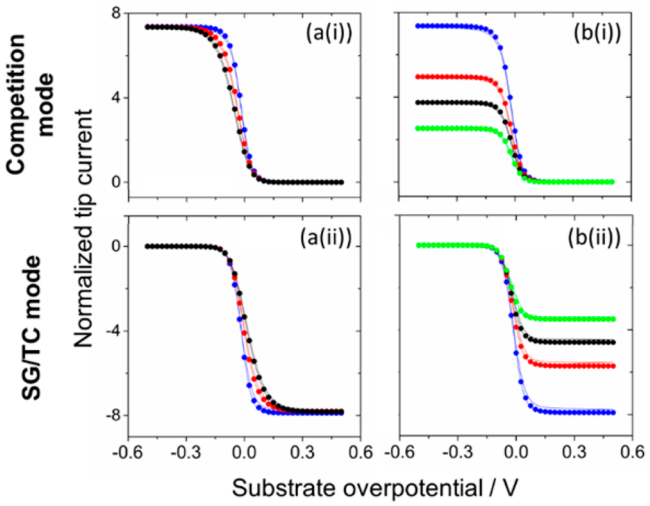

Figure 7. Simulated nanogap substrate voltammetry SECM tip current−substrate potential responses in competition (i) and SG/TC (ii) modes showing the effects of (a) substrate ET kinetics on the shape of the voltammograms (10 cm s^{-1} (blue), 1 cm s^{-1} (red), and 0.5 cm s^{-1} (black)) at L = 0.1 and (b) tip−substrate separation (50 nm (blue), 75 nm (red), 100 nm (black), and 150 nm (green)) for k^0_{HOPG} = 5 cm s^{-1}. Dotted lines represent the analytical adsorption-free fitting where parameters are summarized in SI section S-9, Table S-2, and Table S-3. All other simulation parameters are identical to those used in Figure 5. Also see SI section S-8.

k^0 values employed, a tip current enhancement of ∼7.3 times (competition mode) and ∼7.9 times (SG/TC mode) with respect to $i_{UME,bulk}$, was observed. The resulting "apparent" tip−substrate separations are 53 and 45 nm for the competition and SG/TC modes, respectively. Analysis of these curves with an adsorption-free analytical model is summarized in SI section S-9 Table S-2, again to illustrate the kinetics and distances derived if a researcher assumed this was a simple redox process. It can be seen that both the competition and SG/TC modes give different distances (see above) and that the SG/TC mode overestimates the kinetics while the competition mode gives an underestimation. Interestingly, this has been seen experimentally,[28] but the effects were attributed to the presence of a contaminant layer.

Figure 7b shows simulated UME tip responses when the tip height, L, is varied (0.1, 0.15, 0.2, and 0.3) with k^0_{HOPG} fixed at 5 cm s^{-1}. Again, these voltammograms fitted well with the adsorption-free analytical model, and the results are summarized in SI section S-9 Table S-3. For all tip−substrate heights considered, a higher k^0 value and a smaller gap was observed in the SG/TC mode compared to the competition mode. k^0 values determined from SG/TC mode curves are overestimated and are close to the maximum kinetic limit of detection. A trend of decreasing k^0 with increasing tip−substrate heights was observed, similar to previous experimental observations,[28] where the trend of slower kinetics was attributed to selective permeability of a contaminant layer on HOPG surfaces toward $FcTMA^{+}$. This work however shows that such a trend can (at least partly) be explained by adsorption phenomena of the redox couple itself.

Lastly, note that the simulated voltammograms (Figure 7) show that these new adsorption processes introduce some hysteresis between the forward and reverse scans in both the competition and SG/TC modes, which has also commonly been seen experimentally in nanogap systems,[28,32] indicating

DOI: 10.1021/acs.analchem.5b04715
Anal. Chem. 2016, 88, 3272−3280

that extraneous redox adsorption phenomena may be widespread in this configuration and need to be clearly quantified if these methods are to be accurately interpreted.

CONCLUSIONS

This work has considered the impact of adsorption phenomena on the SECM substrate electrode and tip (insulating support) with several significant outcomes. First, we have shown that substrate voltammetry SECM can be used to quantify adsorption of a redox couple at a substrate electrode. Such effects can readily be seen by changing the voltammetric scan rate applied to the substrate electrode, to achieve a non-steady-state response. Second, we have shown the importance of understanding surface adsorption effects on the glass that surrounds the UME tip, particularly in nanogap voltammetric measurements. The increased surface area-to-solution volume ratio of nanogap experiments makes understanding the adsorption properties of the surface probe essential in order to extract reliable kinetic data, especially if the electrode kinetics are fast (close to the diffusion limit).

We have developed a holistic model for SECM that carefully considers the unequal diffusivities of $FcTMA^+$ and $FcTMA^{2+}$, herein, and the adsorption of the reactant, $FcTMA^+$, onto the HOPG substrate. The adsorption of highly charged $FcTMA^{2+}$ species onto the insulating glass sheath that encapsulates the UME was also considered along with direct ET between $FcTMA^+$ in solution and glass-bound $FcTMA^{2+}$, which significantly affects the magnitude of the limiting current measured. The implication of these findings has been discussed for the case where a researcher would be unaware of such surface adsorption effects and would analyze the response purely in terms of ET kinetics at the substrate electrode. The effects discussed lead to incorrect kinetic parameters, underestimation in the competition mode, and overestimation in the SG/TC mode, as well as incorrect thermodynamic assignments.

For some of the nanogap electrode dimensions considered here, it is possible that other effects such as from the electrical double layer (EDL) will come into play and cannot be ignored. Recently, White et al.[32] showed that limiting currents can be strongly affected (reduced) by the EDL at cell thickness ≤ 100 nm even for typical supporting electrolyte concentrations (200 mM) where the EDL is usually assumed to have negligible effect on mass transport. This work also found hysteresis in voltammograms taken at slow scan rates, with a slight variability of the experimental voltammetric responses at low electrolyte concentrations and at thin cell thicknesses, attributed to the adsorption of $FcTMA^+$ at the Pt electrode surface.[32] There are further effects, such as ion transport in nanogap geometries, that also need further consideration in order to fully understand the SECM nanogap configuration.

ASSOCIATED CONTENT

Supporting Information

The Supporting Information is available free of charge on the ACS Publications website at DOI: 10.1021/acs.analchem.5b04715.

Additional experimental details, cyclic voltammetry at highly oriented pyrolytic graphite, simulated SECM voltammograms for a 12.5 μm radius UME tip, determination of the diffusion coefficients of $FcTMA^+$ and $FcTMA^{2+}$, cyclic voltammetry at "aged" highly oriented pyrolytic graphite electrodes, determination of $FcTMA^+$ and $FcTMA^{2+}$ adsorption on glass, additional simulation details, and kinetic analysis of nanogap SECM simulations (PDF)

AUTHOR INFORMATION

Corresponding Author

*E-mail: p.r.unwin@warwick.ac.uk.

Notes

The authors declare no competing financial interest.

ACKNOWLEDGMENTS

We thank the European Research Council (Grant ERC-2009-AdG 247143-QUANTIF) together with the Monash-Warwick Strategic Funding Initiative for financial support. We also thank Dr. Anatolii S. Cuharuc for helpful advice on finite-element simulations.

REFERENCES

(1) Marcus, R. A. *Annu. Rev. Phys. Chem.* **1964**, *15*, 155.
(2) Gosavi, S.; Marcus, R. A. *J. Phys. Chem. B* **2000**, *104*, 2067−2072.
(3) Chen, S.; Liu, Y.; Chen, J. *Chem. Soc. Rev.* **2014**, *43*, 5372−5386.
(4) Forster, R. J.; Faulkner, L. R. *J. Am. Chem. Soc.* **1994**, *116*, 5444−5452.
(5) Forster, R. J. *Langmuir* **1995**, *11*, 2247−2255.
(6) Forster, R. J. *Anal. Chem.* **1996**, *68*, 3143−3150.
(7) Chidsey, C. E. D.; Murray, R. W. *Science* **1986**, *231*, 25−31.
(8) Chidsey, C. E. D. *Science* **1991**, *251*, 919−922.
(9) Bard, A. J.; Mirkin, M. V.; Unwin, P. R.; Wipf, D. *J. Phys. Chem.* **1992**, *96*, 1861−1868.
(10) Macpherson, J. V.; Marcar, S.; Unwin, P. R. *Anal. Chem.* **1994**, *66*, 2175−2179.
(11) Macpherson, J. V.; Jones, C. E.; Unwin, P. R. *J. Phys. Chem. B* **1998**, *102*, 9891−9897.
(12) Amemiya, S.; Bard, A. J.; Fan, F.-R. F.; Mirkin, M. V.; Unwin, P. R. *Annu. Rev. Anal. Chem.* **2008**, *1*, 95−131.
(13) Aoki, K. *Electroanalysis* **1993**, *5*, 627−639.
(14) Forster, R. J. *Chem. Soc. Rev.* **1994**, *23*, 289−297.
(15) Martin, R. D.; Unwin, P. R. *J. Electroanal. Chem.* **1995**, *397*, 325−329.
(16) Macpherson, J. V.; Beeston, M. A.; Unwin, P. R.; Hughes, N. P.; Littlewood, D. *J. Chem. Soc., Faraday Trans.* **1995**, *91*, 1407−1410.
(17) Sun, P.; Laforge, F. O.; Mirkin, M. V. *Phys. Chem. Chem. Phys.* **2007**, *9*, 802−823.
(18) Mirkin, M. V.; Nogala, W.; Velmurugan, J.; Wang, Y. *Phys. Chem. Chem. Phys.* **2011**, *13*, 21196−21212.
(19) Unwin, P. R.; Bard, A. J. *J. Phys. Chem.* **1991**, *95*, 7814−7824.
(20) Zhang, B.; Fan, L.; Zhong, H.; Liu, Y.; Chen, S. *J. Am. Chem. Soc.* **2013**, *135*, 10073−10080.
(21) Cox, J. T.; Zhang, B. *Annu. Rev. Anal. Chem.* **2012**, *5*, 253−272.
(22) Sun, P.; Mirkin, M. V. *Anal. Chem.* **2006**, *78*, 6526−6534.
(23) Heller, I.; Kong, J.; Heering, H. A.; Williams, K. A.; Lemay, S. G.; Dekker, C. *Nano Lett.* **2005**, *5*, 137−142.
(24) Dumitrescu, I.; Unwin, P. R.; Macpherson, J. V. *Chem. Commun.* **2009**, 6886−6901.
(25) Dudin, P. V.; Snowden, M. E.; Macpherson, J. V.; Unwin, P. R. *ACS Nano* **2011**, *5*, 10017−10025.
(26) Güell, A. G.; Meadows, K. E.; Dudin, P. V.; Ebejer, N.; Macpherson, J. V.; Unwin, P. R. *Nano Lett.* **2014**, *14*, 220−224.
(27) Nioradze, N.; Kim, J.; Amemiya, S. *Anal. Chem.* **2011**, *83*, 828−835.
(28) Nioradze, N.; Chen, R.; Kurapati, N.; Khvataeva-Domanov, A.; Mabic, S.; Amemiya, S. *Anal. Chem.* **2015**, *87*, 4836−4843.
(29) Mampallil, D.; Mathwig, K.; Kang, S.; Lemay, S. G. *Anal. Chem.* **2013**, *85*, 6053−6058.
(30) Mampallil, D.; Mathwig, K.; Kang, S.; Lemay, S. G. *J. Phys. Chem. Lett.* **2014**, *5*, 636−640.

DOI: 10.1021/acs.analchem.5b04715
Anal. Chem. 2016, 88, 3272−3280

(31) Fan, L.; Liu, Y.; Xiong, J.; White, H.; Chen, S. *ACS Nano* **2014**, *8*, 10426−10436.
(32) Xiong, J.; Chen, Q.; Edwards, M. A.; White, H. S. *ACS Nano* **2015**, *9*, 8520−8529.
(33) Byers, J. C.; Nadappuram, B. P.; Perry, D.; Mckelvey, K.; Colburn, A. W.; Unwin, P. R. *Anal. Chem.* **2015**, *87*, 10450−10456.
(34) Mirkin, M. V.; Bard, A. J. *Anal. Chem.* **1992**, *64* (18), 2293−2302.
(35) Chang, J.; Leonard, K. C.; Cho, S. K.; Bard, A. J. *Anal. Chem.* **2012**, *84*, 5159−5163.
(36) Lazenby, R. A.; McKelvey, K.; Peruffo, M.; Baghdadi, M.; Unwin, P. R. *J. Solid State Electrochem.* **2013**, *17*, 2979−2987.
(37) Nioradze, N.; Chen, R.; Kim, J.; Shen, M.; Santhosh, P.; Amemiya, S. *Anal. Chem.* **2013**, *85*, 6198−6202.
(38) Oldham, K. *Anal. Chem.* **1992**, *64*, 646−651.
(39) Zhang, B.; Galusha, J.; Shiozawa, P. G.; Wang, G.; Bergren, A. J.; Jones, R. M.; White, R. J.; Ervin, E. N.; Cauley, C. C.; White, H. S. *Anal. Chem.* **2007**, *79*, 4778−4787.
(40) Penner, R. M.; Heben, M. J.; Longin, T. L.; Lewis, N. S. *Science* **1990**, *250*, 1118−1121.
(41) Shao, Y.; Mirkin, M. V.; Fish, G.; Kokotov, S.; Palanker, D.; Lewis, A. *Anal. Chem.* **1997**, *69*, 1627−1634.
(42) Li, Y.; Bergman, D.; Zhang, B. *Anal. Chem.* **2009**, *81*, 5496−5502.
(43) Nogala, W.; Velmurugan, J.; Mirkin, M. V. *Anal. Chem.* **2012**, *84*, 5192−5197.
(44) Dumitrescu, I.; Dudin, P. V.; Edgeworth, J. P.; Macpherson, J. V.; Unwin, P. R. *J. Phys. Chem. C* **2010**, *114*, 2633−2639.
(45) Lee, H. B. R.; Baeck, S. H.; Jaramillo, T. F.; Bent, S. F. *Nano Lett.* **2013**, *13*, 457−463.
(46) Kang, S.; Mathwig, K.; Lemay, S. G. *Lab Chip* **2012**, *12*, 1262−1267.
(47) Kätelhön, E.; Krause, K. J.; Mathwig, K.; Lemay, S. G.; Wolfrum, B. *ACS Nano* **2014**, *8* (5), 4924−4930.
(48) Zevenbergen, M. A. G.; Singh, P. S.; Goluch, E. D.; Wolfrum, B. L.; Lemay, S. G. *Anal. Chem.* **2009**, *81*, 8203−8212.
(49) Singh, P. S.; Chan, H.-S. M.; Kang, S.; Lemay, S. G. *J. Am. Chem. Soc.* **2011**, *133*, 18289−18295.
(50) Hubbard, A. T.; Anson, F. C. *J. Electroanal. Chem.* **1965**, *9*, 163−164.
(51) Hubbard, A. T.; Anson, F. C. *Anal. Chem.* **1966**, *38*, 1601−1603.
(52) Hubbard, A. T.; Osteryoung, R. A.; Anson, F. C. *Anal. Chem.* **1966**, *38*, 692−697.
(53) Chen, R.; Nioradze, N.; Santhosh, P.; Li, Z.; Surwade, S. P.; Shenoy, G. J.; Parobek, D. G.; Kim, M. A.; Liu, H.; Amemiya, S. *Angew. Chem., Int. Ed.* **2015**, *54*, 15134−15137.
(54) Bond, A. M.; Mclennan, E. A.; Stojanovic, R. S.; Thomas, F. G. *Anal. Chem.* **1987**, *59*, 2853−2860.
(55) Cuharuc, A. S.; Zhang, G.; Unwin, P. R. *Phys. Chem. Chem. Phys.* **2016**, *18*, 4966.
(56) Martin, R. D.; Unwin, P. R. *J. Electroanal. Chem.* **1997**, *439*, 123−136.
(57) Martin, R. D.; Unwin, P. R. *Anal. Chem.* **1998**, *70*, 276−284.
(58) Patten, H. V.; Meadows, K. E.; Hutton, L. A.; Iacobini, J. G.; Battistel, D.; McKelvey, K.; Colburn, A. W.; Newton, M. E.; MacPherson, J. V.; Unwin, P. R. *Angew. Chem., Int. Ed.* **2012**, *51*, 7002−7006.
(59) Baer, C. D.; Stone, N. J.; Sweigart, D. a. *Anal. Chem.* **1988**, *60*, 188−191.
(60) Patel, A. N.; Collignon, M. G.; O'Connell, M. a.; Hung, W. O. Y.; McKelvey, K.; MacPherson, J. V.; Unwin, P. R. *J. Am. Chem. Soc.* **2012**, *134*, 20117−20130.
(61) Patel, A. N.; Tan, S.; Unwin, P. R. *Chem. Commun.* **2013**, *49*, 8776−8778.
(62) Guell, A. G.; Cuharuc, A. S.; Kim, Y.-R.; Zhang, G.; Tan, S.; Ebejer, N.; Unwin, P. R. *ACS Nano* **2015**, *9*, 3558−3571.
(63) Zhang, G.; Cuharuc, A. S.; Güell, A. G.; Unwin, P. R. *Phys. Chem. Chem. Phys.* **2015**, *17*, 11827−11838.
(64) McKelvey, K.; Edwards, M. A.; Unwin, P. R. *Anal. Chem.* **2010**, *82*, 6334−6337.
(65) McKelvey, K.; Snowden, M. E.; Peruffo, M.; Unwin, P. R. *Anal. Chem.* **2011**, *83*, 6447−6454.
(66) Eckhard, K.; Chen, X.; Turcu, F.; Schuhmann, W. *Phys. Chem. Chem. Phys.* **2006**, *8*, 5359−5365.
(67) Unwin, P. R.; Bard, A. J. *Anal. Chem.* **1992**, *64*, 113−119.
(68) Zhang, J.; Slevin, C. J.; Morton, C.; Scott, P.; Walton, D. J.; Unwin, P. R. *J. Phys. Chem. B* **2001**, *105*, 11120−11130.
(69) Zhang, J.; Unwin, P. R. *J. Am. Chem. Soc.* **2002**, *124*, 2379−2383.
(70) O'Mullane, A. P.; Macpherson, J. V.; Unwin, P. R.; Cervera-Montesinos, J.; Manzanares, J. A.; Frehill, F.; Vos, J. G. *J. Phys. Chem. B* **2004**, *108*, 7219−7227.
(71) Whitworth, A. L.; Mandler, D.; Unwin, P. R. *Phys. Chem. Chem. Phys.* **2005**, *7*, 356−365.
(72) Hauquier, F.; Ghilane, J.; Fabre, B.; Hapiot, P. *J. Am. Chem. Soc.* **2008**, *130*, 2748−2749.

DOI: 10.1021/acs.analchem.5b04715
Anal. Chem. 2016, 88, 3272−3280